Supplementary information

1. Chemicals

All chemicals were used as received unless otherwise specified. [BMIm][BF_4] ≥ 98% (CAS: 174501-65-6) and hexylamine 99% (CAS: 111-26-2) were purchased from Sigma Aldrich. The hydrophobized spherical silica nanoparticles were synthesized according to the optimized protocol described below. Trimethoxysilane 95% (CAS: 2487-90-3), [BMIm][BF_4] 98%+ (CAS: 174501-65-6), TEOS 99.9% (CAS: 78-10-4) and dimethyldichlorosilane 99+% (CAS: 75-78-5) were sourced from Thermo Scientific. Toluene ≥ 99.8% (CAS: 108-88-3), methanol ≥ 99.8% (CAS: 67-56-1), and acetone ≥ 99.8% (CAS: 67-64-1) were purchased from Fisher Chemical. Ammonia 25% (CAS: 1336-21-6) was sourced from Merck. Absolute anhydrous ethanol (CAS: 64-17-5) was purchased from Carlo Erba. Ammonia 20.5% (CAS: 1336-21-6) and hydrochloric acid 37% (CAS: 7647-01-0) were obtained from VWR Chemicals. The 1 $mol \cdot L^{-1}$ hydrochloric acid solution was prepared by diluting 37% hydrochloric acid with deionized water. Deionized water was obtained using an ELGA PURELAB Option Q system.

2. Experimental

2.1. Preparation of spherical silica nanoparticles

243 mL of absolute ethanol, 5.64 mL of 25% ammonia, and 32.5 mL of deionized water were added to a 500 mL flask and vigorously stirred for 15 minutes at 70 °C in an oil bath using a magnetic stir bar and a magnetic stirrer. 18.8 mL of TEOS were then rapidly added dropwise to the mixture, which was stirred for 2 h, after first reducing the stirring speed until there was almost no surface turbulence (around 100–150 rpm). The resulting colloidal suspension was transferred into 50 mL centrifuge tubes and centrifuged at 12000 rpm for 10 min at 10 °C. The supernatant was removed, and the nanoparticles were redispersed with 20 mL of absolute ethanol in each tube using an ultrasonic bath. The resulting colloidal suspensions were centrifuged again at 12000 rpm for 10 min at 10 °C. The ultrasound redispersion and centrifugation steps were repeated a second time to thoroughly wash the nanoparticles. After the final centrifugation, as much supernatant as possible was removed, and the nanoparticles were dried overnight in a vacuum oven (50 °C, 9 mbar).

2.2. Surface modification of spherical silica nanoparticles

The previously synthesized nanoparticles (4.8 g) were added to a 250 mL flask with 142 mL of toluene and dispersed using an ultrasonic bath for 30 min. The mixture was then placed in an oil bath and vigorously stirred for 15 min at 60 °C using a magnetic stir bar and a magnetic stirrer. During this time, the flask was also purged with nitrogen. While maintaining the nitrogen purge, 3.8 mL of hexylamine followed by 1.75 mL of dimethyldichlorosilane were added dropwise. The nitrogen purge was then stopped, the flask was sealed with a stopper, and the reaction mixture was vigorously stirred for 4 h at 60 °C. The resulting colloidal suspension was transferred to 50 mL centrifuge tubes and centrifuged at 12000 rpm for 10 min at 10 °C. The supernatant was removed, and the nanoparticles were redispersed in 20 mL of toluene using an ultrasonic bath. The colloidal suspension was centrifuged again at 12000 rpm for 10 min at 10 °C. These redispersion and centrifugation steps were repeated a second time, but this time using 20 mL of a 1:1 toluene/methanol mixture to facilitate redispersion. After the final centrifugation, the supernatant was removed as completely as possible, and the nanoparticles were dried overnight in a vacuum oven (50 °C, 9 mbar).

2.3. Characterization of silica nanoparticles

The nanoparticle size distribution was determined by DLS using a Malvern Panalytical Zetasizer Nano ZS (Figure S1). To confirm their physical diameter, the nanoparticles were also examined using SEM with a Jeol JSM-IT-800 microscope operated via the SEM Center software (Figure S2). Particle diameters were determined from the SEM micrographs using a dedicated macro in ImageJ. A spatula tip of nanoparticles was dispersed in 2 mL of methanol; subsequently, a drop of this colloidal dispersion was dispersed in 2 mL of methanol and analyzed by DLS. For SEM imaging, a small amount of nanoparticles was deposited onto an SEM stub coated with double-sided carbon tape using the tip of a spatula. Excess material was removed by gently tapping the stub. The nanoparticles have an average diameter of approximately 80 nm.

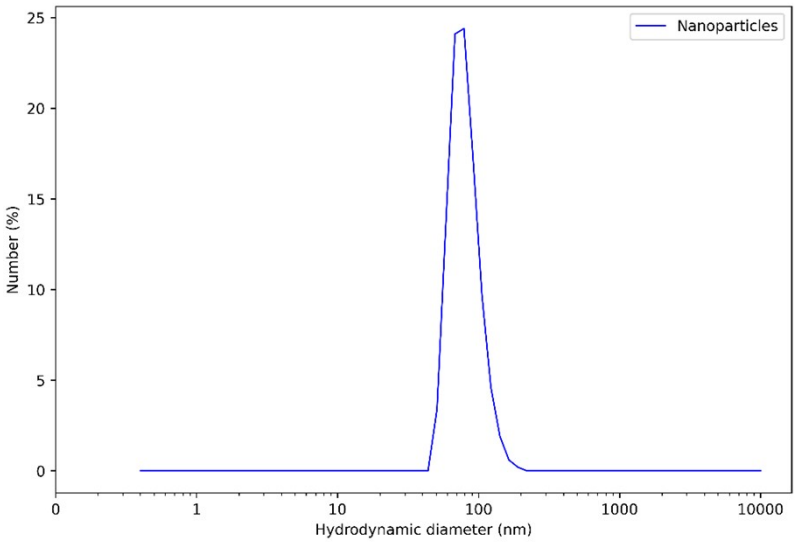

Figure S1. Size distribution of spherical silica nanoparticles after surface modification in DLS.

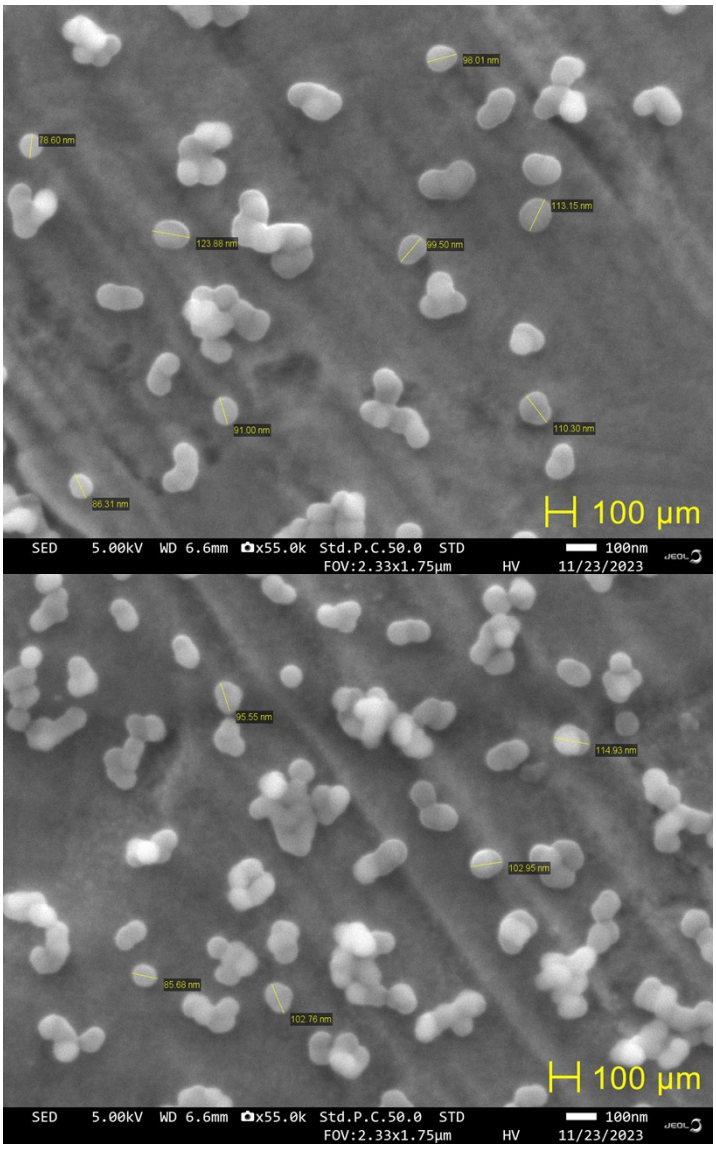

Figure S2. SEM images of nanoparticles

The difference between the nanoparticles before and after surface modification was characterized using several methods. First, visual characterization was performed by dispersing the nanoparticles—both before and after surface modification—in deionized water using an ultrasonic bath (Figure S3).

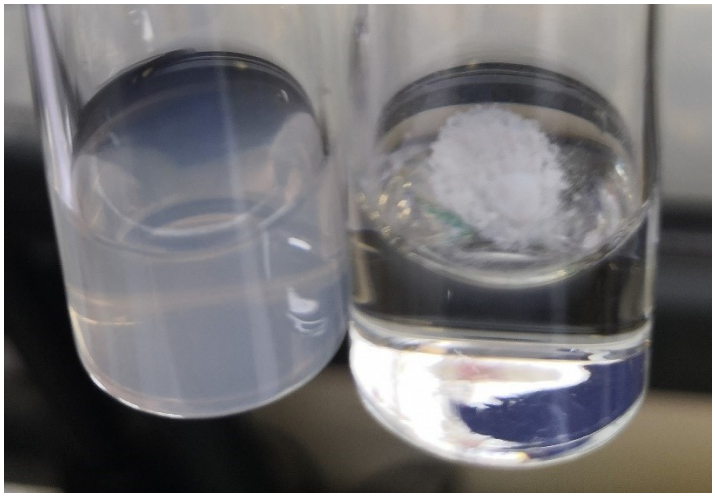

Figure S3. Nanoparticles before (left) and after surface modification (right) dispersed by ultrasound in deionized water.

A colloidal suspension was obtained with the nanoparticles prior to surface modification, whereas the modified nanoparticles could not be wetted. Subsequently, the nanoparticles were analyzed using more quantitative techniques: FTIR, TGA, ^{29}Si solid-state MAS NMR, and ^{29}Si solid-state CP-MAS ^{1}H → ^{29}Si NMR. The only analytical method sensitive enough to detect a difference between the nanoparticles before and after surface modification was ^{29}Si solid-state CP-MAS ^{1}H → ^{29}Si NMR (Figure S4).

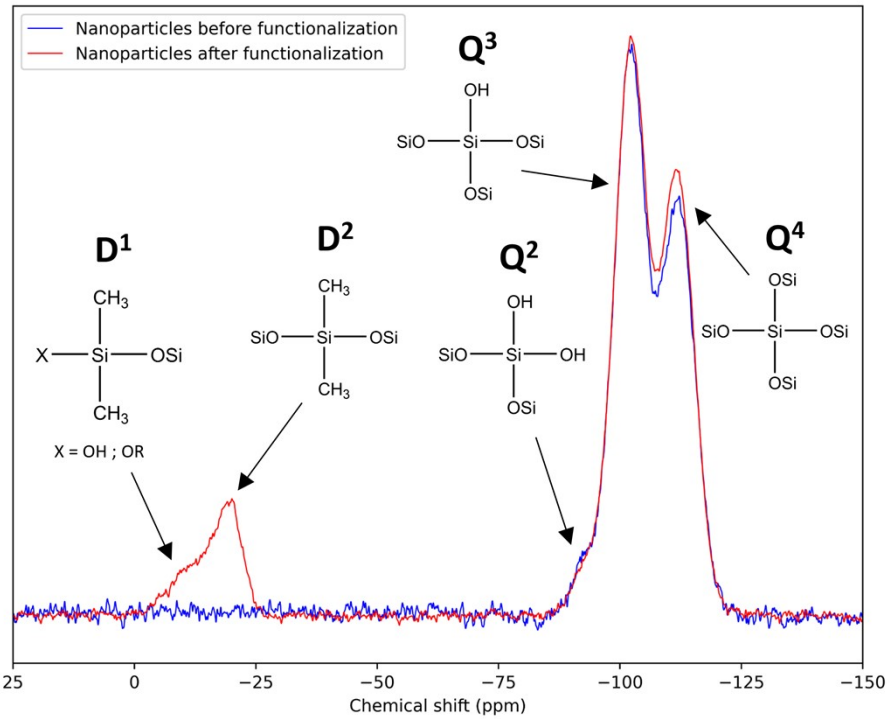

Figure S4. ^{29}Si solid-state CP-MAS ^{1}H → ^{29}Si NMR spectra of silica nanoparticles before/after functionalization

Unfortunately, this is a qualitative rather than a quantitative method. The appearance of two peaks between 0 and -25 ppm can be observed on the NMR spectrum, corresponding to the D^1 and D^2 signals associated with the functionalization introduced by the reaction between dichlorodimethylsilane and surface Si-OH groups.

2.4. Choosing the size of nanoparticles

The selection of nanoparticle size represents a trade-off between the quantity required to prepare the Pickering emulsion and the mesoporous volume induced by the voids between nanoparticles, which hinders the characterization of the pore volume of the capsules' silica shell. The minimum theoretical mass of nanoparticles required to cover all emulsion droplets with a monolayer of spherical nanoparticles arranged in a hexagonal close packing structure is:

$$m_p = \frac{4C\rho_p d_p V_d}{sin^2(\theta) d_g}$$

where m_p is the mass of the nanoparticles (kg), ρ_p is the nanoparticle density (2200 kg.m^{-3} for silica), d_p is the average nanoparticle diameter (m), V_d is the dispersed phase volume (4.285 $\times$ 10^{-6} m^3), θ is the contact angle (radians), d_g is the average emulsion droplet diameter (15 µm), and C is a correction factor for nanoparticle surface coverage on the emulsion droplets, equal to 0.91 in the case of hexagonal close packing.

The only parameter in this equation dependent on the surface functionalization of the nanoparticles is the contact angle. Since this value was not measured, the quantity of nanoparticles required is plotted as a function of the contact angle in Figure S5 for two different nanoparticle sizes: 80 nm (the nanoparticles used in this study) and 200 nm. The latter corresponds to a size slightly larger than that calculated in the paper to ensure a pore size induced by interparticle voids greater than 50 nm.

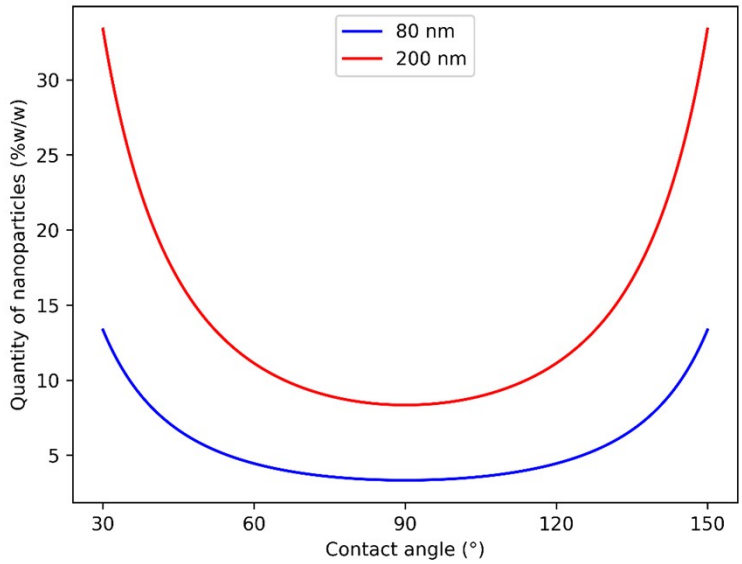

Figure S5. Quantity of spherical nanoparticles required (in %w/w relative to the dispersed phase) as a function of contact angle to cover all emulsion droplets with a hexagonal close-packed monolayer of nanoparticles, for two different nanoparticle sizes.

The nanoparticle quantity ranges from 3.6 to 14.2%w/w for the 80 nm nanoparticles (the 7%w/w used in this study falls within this theoretical range), whereas between 8.3 and 33.3%w/w is required for 200 nm nanoparticles. If the 200 nm nanoparticles follow the same trend as the 80 nm ones, 16%w/w would be required to stabilize the Pickering emulsion. Since using such a large amount of nanoparticles is impractical, the 80 nm nanoparticles were selected, despite their inherent mesoporosity between 12 and 50 nm, which hinders the investigation of the capsule mesoporosity in this range.

2.4. Synthesis of the capsules

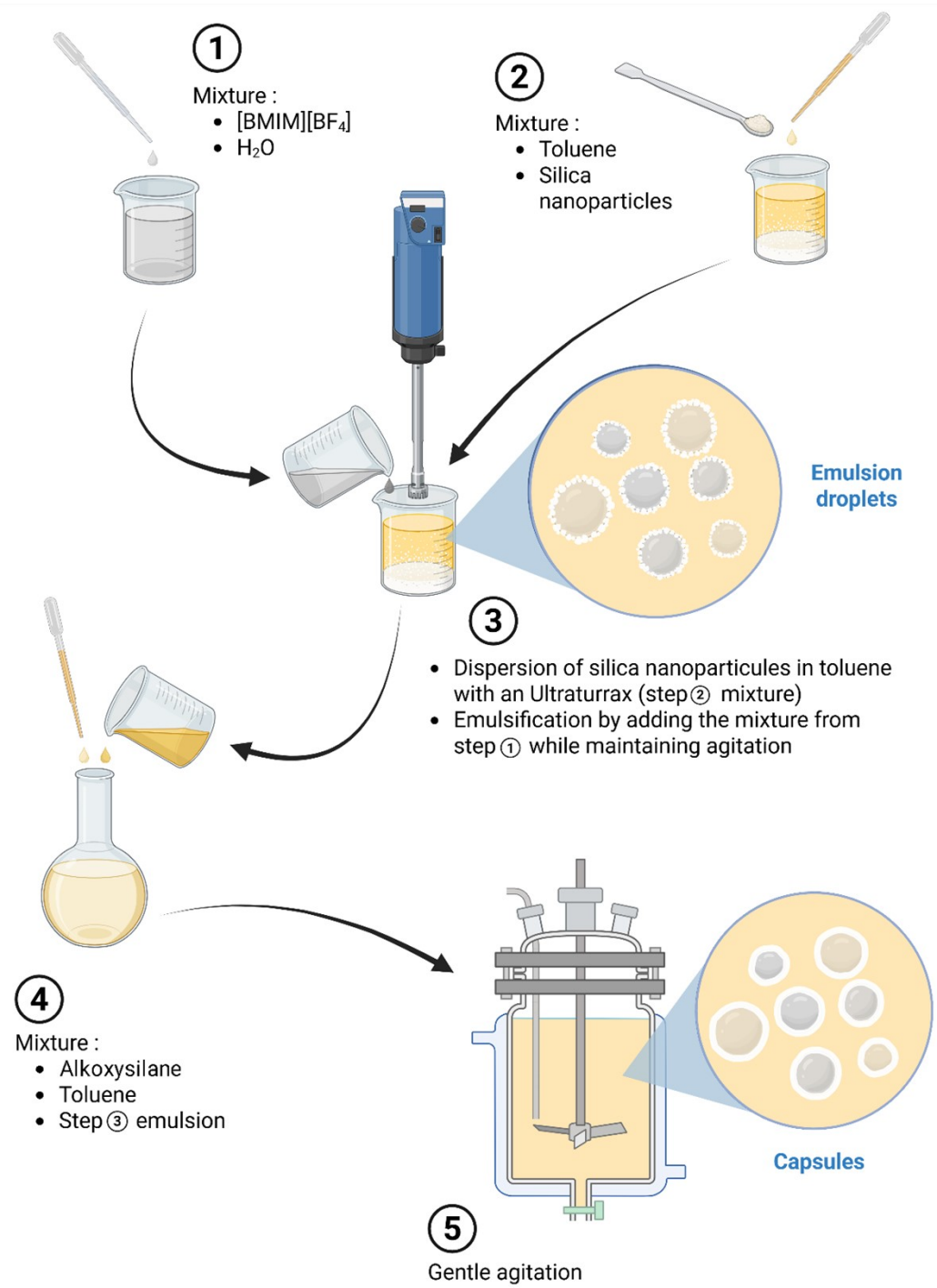

Figure S6. Summary diagram of capsule synthesis

Table S1. Experimental conditions for capsule syntheses.

Experiments	[BMIm][BF_4] (g)	Aqueous solution (g)	Nanoparticles (g)	TMS (g)	Reaction time (h)	Temperature (°C)
RD1	4.93	H_2O 0.22	0.37	0.37	6	5
RD2	4.94	H_2O 0.22	0.37	0.37	6	20
RD3	4.92	H_2O 0.22	0.41	0.37	6	50
RD4	4.94	H_2O 0.22	0.38	0.37	24	20
RD5	4.93	HCl 1M 0.22	0.36	0.37	6	20
RD6	4.94	$NH_{3(aq)}$ 20.5% 0.22	0.38	0.36	6	20
RD7	4.93	H_2O 0.23	0.36	2.91	6	20
RD8	4.15	H_2O 0.86	0.37	0.37	6	20

2.5. Reproducibility of the analysis of textural properties via nitrogen physisorption

A single batch of capsules was analyzed via nitrogen physisorption with an interval of several days to assess the reproducibility of the textural property analysis. The corresponding nitrogen isotherms are presented in Figure S7, the micropore and mesopore size distributions in Figure S8, and the summarized textural properties in Table S2.

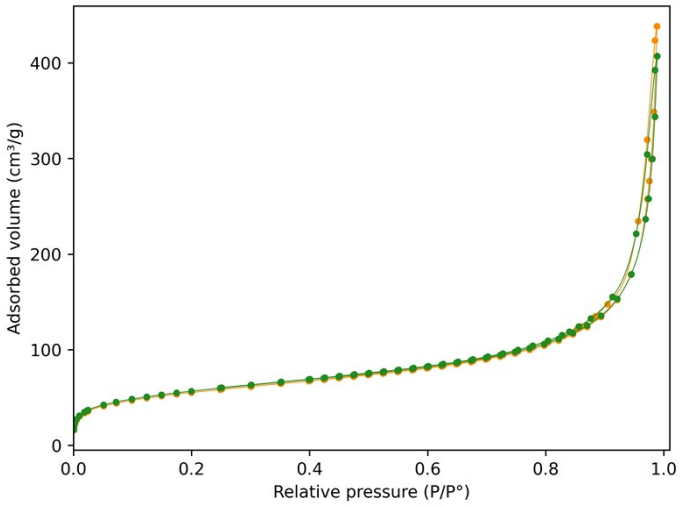

Figure S7. Nitrogen physisorption isotherms of a single batch of capsules analyzed several days apart.

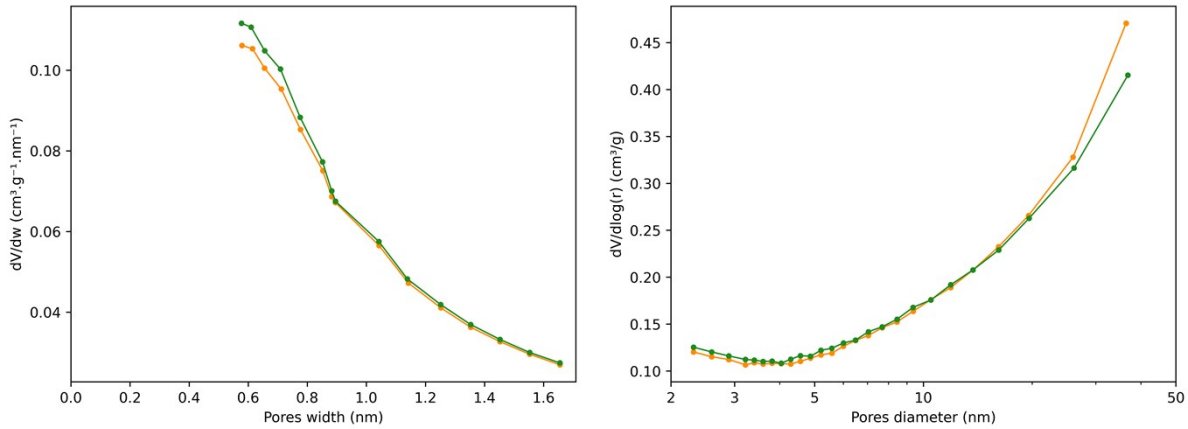

Figure S8. Size distributions of micropores (left) and mesopores (right) of a single batch of capsules analyzed several days apart.

Table S2. Textural properties of of a single batch of capsules analyzed several days apart.

Sample	S_{BET} (m^2/g)	V_{meso} (cm^3/g)	V_{micro} (cm^3/g)
Orange	201	0.356	0.086
Green	206	0.321	0.088

2.6. Supercritical CO_2 drying

Capsules are inserted into the custom sample holder (Figure S9), which is then added into the chamber of the supercritical dryer. Acetone is added until the sample holder was completely submerged. The drying chamber was then closed and cooled to 10 °C (the chamber must be at least 7 °C cooler than the liquid CO_2 cylinder to allow the fluid to enter the chamber). Twelve successive washes were then performed, each time emptying 50% of the liquid volume from the chamber and refilling it with liquid CO_2. After each refill, a pause of 2–3 minutes was observed to allow the liquid CO_2 to homogenize within the sample holder. Once all exchanges were completed, the chamber was filled one last time with liquid CO_2 and then heated to 37 °C. Pressure was automatically regulated by the device and stabilized around 80 bar to remain above the critical pressure and temperature required for the supercritical state of CO_2. Once 37 °C and 80 bar were reached, the chamber was depressurized in a controlled manner at 0.5 bar·min^{-1} until atmospheric pressure was reached.

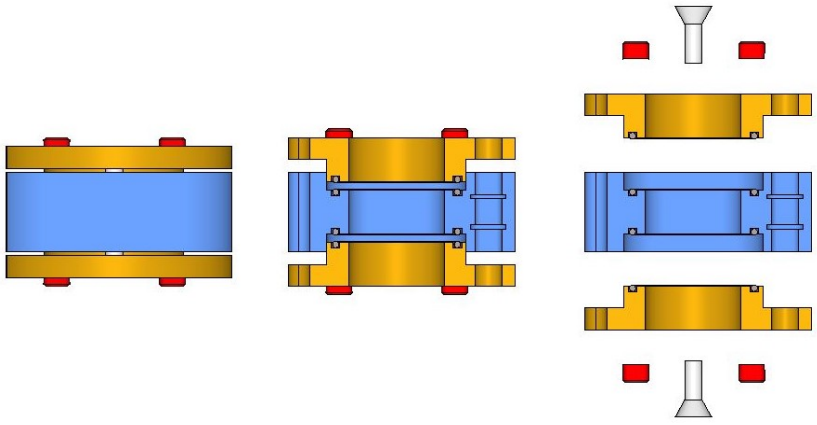

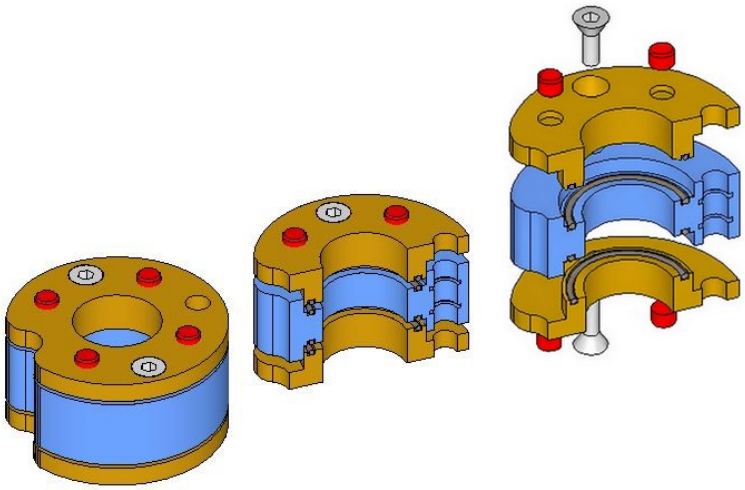

Figure S9. Schemes of the custom sample holder

3. Characterization

3.1. Optical microscopy

The capsules were observed after first diluting the dispersion obtained at the end of the synthesis. Two solvents were used for this purpose: dodecane and toluene. Dodecane is much less volatile than toluene at room temperature and atmospheric pressure, which makes it suitable for microscope setup prior to observations with toluene. Observations in toluene were ultimately chosen because they are more representative of the actual conditions, and the images are clearer and cleaner than those obtained with dodecane, allowing for better contour detection using the Python script. The same protocol was followed for each solvent: approximately 1 mL of solvent was added to a small vial, followed by 10–15 drops of the capsule dispersion. The mixture was gently shaken by hand, and a few drops were then placed on a microscope slide. An example of an optical microscopy observation and the corresponding distribution obtained from this observation is shown in Figure S10.

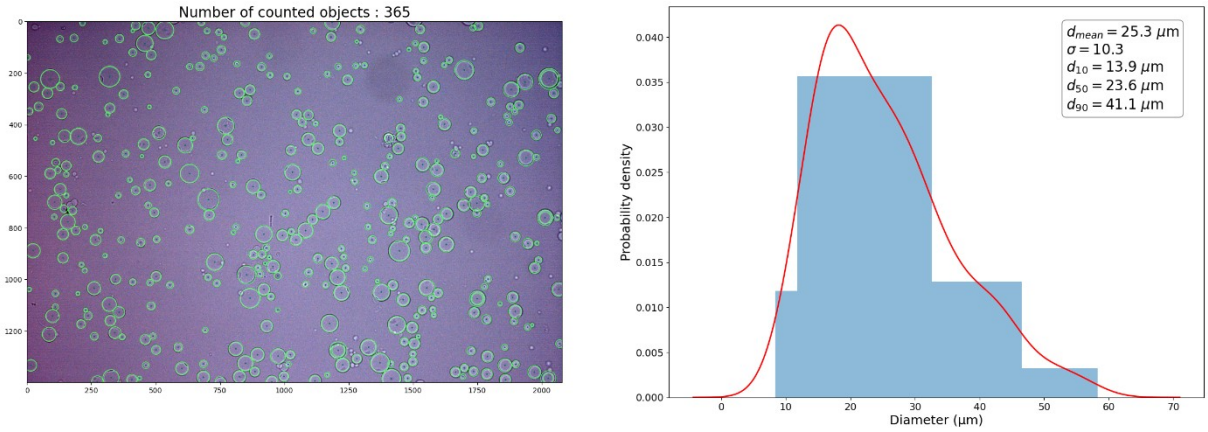

Figure S10. Size distribution of capsules from an optical microscopy image.

Histogram bins' widths were chosen arbitrarily using a Bayesian blocks binning. This method dynamically optimizes bin widths based on local data density—yielding narrower bins in highly populated regions for greater precision, and wider bins in sparse regions to reduce visual noise and prevent over-binning. The heights represent the actual probability density. Second, regarding the thin red line and the distribution type: The red line represents a non-parametric probability density estimation modeled using a Fast Fourier Transform Kernel Density Estimation (FFTKDE). We applied a Gaussian kernel with a bandwidth optimized by the Silverman or Improved Sheather-Jones algorithms. We deliberately chose this non-parametric KDE approach over a forced lognormal fit because it more accurately captures the true, empirical distribution of the capsules, which can sometimes exhibit slight asymmetries or subtle multimodality that a strict lognormal model would smooth over.

3.2. Nitrogen physisorption

Nitrogen physisorption allows probing pore sizes ranging from 0.4 nm to 50 nm. This gas adsorption technique involves introducing a known volume of N_2 (adsorbate) to a solid material in a sample chamber at a temperature of 77 K (the boiling point of N_2). At this temperature, a specific number of gas molecules adsorb onto the surface of the solid via van

der Waals forces. N_2 is added in a series of controlled doses, and the pressure in the sample chamber is measured after each dose. The ideal gas law can then be used to determine the volume of gas adsorbed by the sample. The resulting relationship between the volume of gas adsorbed and the relative pressure at constant temperature is known as an isotherm (either adsorption or desorption). Determining the textural properties of the capsules using nitrogen physisorption (as well as mercury porosimetry) requires prior treatment of the samples. The capsules were degassed by heating under high vacuum (approximately 5×10^{-6} mbar) for 24 h before analysis. The type of isotherm and the hysteresis loop were identified based on a technical report from IUPAC[1].

Several well-established methods from the literature were used to determine the specific surface area, microporous and mesoporous volumes, and pore size distribution. All calculations and details of the methods used are provided in the following sections.

BET method: The specific surface area developed by the material was calculated using the Brunauer–Emmett–Teller (BET) method. This method, based on Langmuir's theory, is primarily applied to type II and IV isotherms[1]. The first step involves converting part of the isotherm into a "BET plot" to deduce the amount of gas adsorbed in the monolayer. The BET equation is as follows:

$$\frac{\frac{P}{P_0}}{V\left(1-\frac{P}{P_0}\right)} = \frac{C-1\,P}{V_m C\,P_0} + \frac{1}{V_m C} \#(1)$$

With V being the adsorbed volume (in $cm^3 \cdot g^{-1}$), P/P_0 the relative pressure, V_m the amount of gas adsorbed in the monolayer (in $cm^3 \cdot g^{-1}$), and C the BET constant. A linear regression is performed on the previous equation within the relative pressure range [0.05; 0.30] according to the following relation:

$$\frac{1}{V\left(\frac{P}{P_0}-1\right)} a\frac{P}{P_0} + b \#(2)$$

It is thus possible to determine, using the slope a and the y-intercept b from the previous linear regression, the values of the factor C and V_m as follows[1]:

$$V_m = \frac{1}{a+b} \quad ; \quad C = 1 + \frac{a}{b} \#(3)$$

The second step consists in calculating the BET specific surface area using the following equation:

$$S_{BET} = \frac{V_m N_A \sigma_m}{v_m} \#(4)$$

where S_{BET} is the BET specific surface area (in $m^2 \cdot g^{-1}$), N_A is Avogadro's number, σ_m is the molecular cross-sectional area of N_2, equal to 1.62×10^{-19} m^2, and v_m is the molar volume of the adsorbed gas, equal to 22400 $cm^3 \cdot mol^{-1}$. In some cases, especially when the adsorbent is

microporous, the transformed BET equation may exhibit multiple linear regions below a relative pressure of 0.35, leading to the calculation of several values for the monolayer capacity[2]. In practice, since it is often difficult to determine a priori whether micropores are present or not, it is simpler to systematically apply the following criteria[2]. These criteria do not affect the result in the absence of micropores, but they ensure reproducibility when micropores are present[2]. The criteria are as follows[1]:

- The C parameter must be positive. A negative C value would be an initial indication that the calculation was not performed within the appropriate pressure range.
- The application of the BET equation must be limited to a pressure range in which the term $V(1 - P/P_0)$ is increasing; if this term is not increasing within the relative pressure interval [0.05; 0.30], it will be necessary to reduce the upper bound of the interval until the term increases.
- The P/P_0 value corresponding to the V_m value on the isotherm must lie within the selected pressure range.

BJH method: The mesoporous volume and the pore size distribution ranging from 2 to 50 nm were calculated using the Barrett-Joyner-Halenda (BJH) method. This method is mainly applied to type IV isotherms, whose saturation plateau is characteristic of a mesoporous adsorbent exhibiting a type H1 or H2 hysteresis loop[3]. It is a generic method because a consensus has been established to assimilate the network of interconnected pores to a set of cylindrical capillaries representing the same volume and surface area as the actual porous network.

This method is based on several assumptions[3]:

- The structure of the material is assumed to be rigid, and the mesopores that compose it are independent and have a well-defined geometry. Given the impossibility of satisfactorily modeling the structure of a real porous network, a consensus has been established to assimilate the network of interconnected pores to a set of cylindrical capillaries representing the same volume and surface area as the actual porous network;
- Multimolecular adsorption occurs on the walls of the mesopores in the same way as on a flat surface;
- The Kelvin equation is assumed to be applicable in mesopores. In the case of cylindrical pores, it is defined as:

$$\ln\left(\frac{P}{P_0}\right) = -\frac{2\gamma v_m^l}{r_K RT}\cos(\theta) \#(5)$$

with γ the surface tension of the liquid (here the adsorbed and condensed gas) on the surface (N·m⁻¹), v_m^l the molar volume of the adsorbate in liquid form (m³·mol⁻¹), r_K the Kelvin radius (m), R the ideal gas constant, T the temperature (K), and θ the liquid/surface contact angle (perfect wetting is assumed, hence $cos(\theta) = 1$). Ideally, $\theta = 0$ when the isotherm ends asymptotically at the saturation line $P/P_0 = 1$. If it intersects this line, strictly speaking $\theta \neq 0$. In the case of N_2 at 77 K, the Kelvin equation is written as:

$$r_K = -\frac{0.415}{\log\left(\frac{P}{P_0}\right)} \#(6)$$

with r_K in nm.

- Capillary condensation occurs in mesopores whose walls are already covered with a multimolecular layer of thickness t, which depends on the equilibrium pressure according to an empirically defined law. Several such laws exist, but the most common is the Harkins and Jura equation, as it is less empirical, defined as:

$$t = \sqrt{\frac{0.1399}{0.034 - \log\left(\frac{P}{P_0}\right)}} \#(7)$$

with t in nm.

- In the case of a cylindrical pore, the pore radius r_p is related to the Kelvin radius by the following relation:
  $r_p = r_K + t \#(8)$

Calculations can be carried out on either the desorption branch or the adsorption branch. They are usually performed on the desorption branch, which is most representative of the equilibrium between the N_2 remaining in the gaseous state and the N_2 condensed by capillary action, particularly with H1 hysteresis loops representing independent and ordered cylindrical pores. In the case of H2 or H3 hysteresis loops, which represent disordered interconnected pores, there is a risk of pore blocking and cavitation; therefore, using the adsorption branch is more appropriate. In the case of capsules and nanoparticles, all the isotherms obtained were type II isotherms with an H3 hysteresis loop, so the adsorption branch was used. The principle of the BJH method is thus based on a discrete analysis of the desorption (or adsorption) branch, starting from the highest relative pressure reached. Intervals of relative pressure are defined, and it is assumed that, at each relative pressure point, the desorbed gas originates partly from the desorption of gas condensed in a certain pore size range (with smaller pore sizes corresponding to lower pressures), and partly from the decrease in the thickness of the adsorbed layer in larger pores that had already been emptied of their condensed gas. The same reasoning can be applied to the adsorption branch.

Given a law to evaluate t, the Kelvin equation, and an assumption about the pore shape, it is then possible to calculate by iteration the wall area and volume of each pore size category. The sum of these values leads to a cumulative specific surface area and a cumulative pore volume. Let $\bar{r}_{p,n}$ be the average mesopore radius at the nth desorption step as defined in[3]:

$$\bar{r}_{p,n} = \frac{r_{p,n} + r_{p,n-1}}{2} \#(9)$$

During the first desorption step, the average mesopore radius $\bar{r}_{p,1}$ is equal to:

$$\overline{r_{p,1}} = \frac{r_{p,1} + r_{p,0}}{2} \#(10)$$

The desorbed quantity δn_1^a corresponds only to the evaporation of the N_2 that was condensed in the first class of mesopores, assumed to be cylindrical. The volume of liquid evaporated is then[3]:

$$\delta v_1^l = v_m^l \delta n_1^a = \pi(\overline{r_{p,1}} - t_1)^2 \delta l_1 \#(11)$$

where δv_1^l is the volume of evaporated liquid (in $cm^3 \cdot g^{-1}$), v_m^l the molar volume of liquid N_2 at 77 K (34.7 $cm^3 \cdot mol^{-1}$), δn_1^a the desorbed amount (in $mol \cdot g^{-1}$), t_1 the thickness of the multimolecular layer at the first relative pressure (in nm), and δl_1 the length of the first class of mesopores. This length can be expressed as a function of $\overline{r_{p,1}}$ and the pore volume of the first class of mesopores as follows[3]:

$$\delta l_1 = \frac{\delta v_{p,1}}{\pi \overline{r_{p,1}^2}} \#(12)$$

with $\delta v_{p,1}$ the pore volume of the first class of mesopores (in $cm^3 \cdot g^{-1}$). It is thus possible to calculate the value of $\delta v_{p,1}$[3]:

$$\delta v_{p,1} = \delta v_1^l \left(\frac{\overline{r_{p,1}}}{\overline{r_{p,1}} - t_1} \right)^2 \#(13)$$

During the second desorption step, the desorbed amount δn_2^a involves not only the evaporation of the N_2 condensed in the second class of mesopores but also the decrease in the thickness of the multimolecular layer remaining adsorbed in the mesopores of the first class[3]. The desorbed liquid volume $\delta v_{t,2}$, linked to the decrease in thickness of the multimolecular layer, is therefore equal to[3]:

$$\delta v_{t,2} = \delta t_2 2\pi(\overline{r_{p,1}} - t_2)\delta l_1 \#(14)$$

with $\delta t_2 = (t_1 - t_2)$ representing the reduction in thickness of the multimolecular layer (in nm). The length of the first class of mesopores δl_1 can be expressed as follows[3]:

$$\delta l_1 = \frac{\delta a_{p,1}}{2\pi \overline{r_{p,1}}} \#(15)$$

with $\delta a_{p,1}$ the surface area of the first class of mesopores (in $m^2 \cdot g^{-1}$). It follows[3]:

$$\delta v_{t,2} = \delta t_2 \delta a_{p,1} \left(1 - \frac{t_2}{\overline{r_{p,1}}} \right) \#(16)$$

The surface area of the first class of mesopores $\delta a_{p,1}$ can be obtained from $\overline{r_{p,1}}$ and the previously calculated pore volume $\delta v_{p,1}$[3]:

$$\delta a_{p,1} = \frac{2\delta v_{p,1}}{\overline{r_{p,1}}} \#(17)$$

The volume of liquid due solely to the evaporation of the condensate in the second class of mesopores is expressed as follows[3]:

$$\delta v_{c,2} = \delta v_{p,2} \left(\frac{\overline{r_{p,2}} - t_2}{\overline{r_{p,2}}} \right)^2 \#(18)$$

with $\delta v_{c,2}$ the volume of liquid due solely to the evaporation of the condensate in the second class of mesopores (in $cm^3 \cdot g^{-1}$), and $\delta v_{p,2}$ the pore volume of the second class of mesopores. The total volume of liquid desorbed in the second step is therefore equal to[3]:

$$\delta v_2^l = \delta v_{c,2} + \delta v_{t,2} = \delta v_{p,2}\left(\frac{\overline{r_{p,2}} - t_2}{\overline{r_{p,2}}}\right)^2 + \delta t_2 \delta a_{p,1}\left(1 - \frac{t_2}{\overline{\overline{r_{p,1}}}}\right) \#(19)$$

The pore volume of the second class of mesopores $\delta v_{p,2}$ is thus equal to[3]:

$$\delta v_{p,2} = \left(\frac{\overline{r_{p,2}}}{\overline{\overline{r_{p,2}} - t_2}}\right)^2\left(\delta v_2^l - \delta t_2 \delta a_{p,1}\left(1 - \frac{t_2}{\overline{\overline{r_{p,1}}}}\right)\right) \#(20)$$

During the third desorption step, the calculations are identical to those of the second step, except that the decrease in the thickness of the multimolecular layer occurs in all the mesopores that have already been emptied of their capillary condensate[3]. The pore volume of the n^{th} desorption step is expressed as[3]:

$$\delta v_{p,n} = \left(\frac{\overline{r_{p,n}}}{\overline{\overline{r_{p,n}} - t_n}}\right)^2\left(\delta v_n^l - \delta t_n \sum_{i=1}^{n-1} \delta a_{p,i}\left(1 - \frac{t_n}{\overline{\overline{r_{p,i}}}}\right)\right) \qquad with\ n > 2 \#(21)$$

Although this method was originally developed for cylindrical pores, it has been widely used for other pore shapes.

HK method: The microporous volume was calculated using the Horvath-Kawazoe (HK) method. This method is used to relate gas adsorption isotherm measurements to the micropore size of an adsorbent. It is slightly more accurate than the BJH method because it allows for the characterization of micropores (< 2 nm) by considering certain properties of the material (adsorbent) and the probe gas (adsorbate), as well as the shape of the pores.

For slit-shaped pores (the case for capsules, as they exhibit type II isotherms with an H3 hysteresis loop), Horvath and Kawazoe established the following equation[4]:

$$\ln\left(\frac{P}{P_0}\right) = \frac{N_A \quad IP}{RT\sigma^4(l-d)}\left(\frac{\sigma^4}{3\left(l - \frac{d}{2}\right)^3} - \frac{\sigma^{10}}{9\left(l - \frac{d}{2}\right)^9} - \frac{\sigma^4}{3\left(\frac{d}{2}\right)^3} + \frac{\sigma^{10}}{9\left(\frac{d}{2}\right)^9}\right) \#(22)$$

where P/P_0 is the relative pressure, N_A is Avogadro's number equal to 6.022×10^{23} mol^{-1}, R is the ideal gas constant, T the temperature (K), and l the distance between the molecular centers of the two opposite walls of the pore (in meters). d corresponds to the sum of the adsorbate and adsorbent diameters and is defined as[4]:

$$d = d_a + d_A \#(23)$$

where d_a is the diameter of an adsorbent atom (m) and d_A the diameter of an adsorbate molecule. σ is the distance between a gas atom and the solid surface at zero interaction energy, defined as[4]:

$$\sigma = \frac{0{,}858d}{2} \#(24)$$

IP is the interaction parameter defined as[4]:

$$IP = N_a A_a + N_A A_A \#(25)$$

where N_a and N_A are the number of molecules per unit area for the adsorbent and adsorbate respectively, and A_a and A_A are the dispersion constants that can be determined using the Kirkwood-Muller equation[4]:

$$A_a = \frac{6mc^2\alpha_a\alpha_A}{\frac{\alpha_a}{\chi_a}+\frac{\alpha_A}{\chi_A}} \#(26) \qquad A_A = \frac{3mc^2\alpha_A\chi_A}{2} \#(27)$$

where m is the mass of an electron (9.109 × 10^{-31} kg), c is the speed of light (2.998 × 10^8 m·s^{-1}), $\alpha_a$and χ_a are the polarizability (m^3) and magnetic susceptibility of an adsorbent atom, α_A and χ_A are the polarizability and magnetic susceptibility (m^3) of an adsorbate molecule. To obtain the most realistic estimate of micropore size, it is necessary to use data from previous calculations for N_2 at 77 K as the adsorbate and silica as the adsorbent. These data and their respective sources are provided in **Table S3**.

Table S3. Physical parameters involved in the calculations of the HK method.

Parameter	**N_2 (adsorbate)**	**SiO_2 (adsorbent)**
Diameter (m)	0.364 × 10^{-9} [5, 6]	0.276 × 10^{-9} [7, 8] [*]
Polarizability (cm^3)	1.740 × 10^{-24} [5, 9]	2.957 × 10^{-24} [**]
Magnetic susceptibility (cm^3)	1.993 × 10^{-29} [9]	4.915 × 10^{-29} [9]
Molecular surface density (molecule.cm^{-2})	6.710 × 10^{14} [5]	1.31 × 10^{15} [***]

[*] Value obtained from the 12-6 Lennard-Jones potential and the Kirkwood-Muller formalism for dispersion forces, using the atomic properties of silicon (Si) and oxygen (O); this value also corresponds to the O–O distance in amorphous silica (in the case of oxides and monolayer adsorption, a common assumption is to consider only the interactions between the oxygen atoms of the oxide and the adsorbate).
[**] Value calculated from the Lorentz–Lorenz equation (see below).
[***] Value calculated from the molecular diameter (see below).

The polarizability α_a of silica was obtained using the Lorentz–Lorenz equation:

$$\frac{n^2-1}{n^2+2} = \frac{4\pi}{3}N\alpha_a \#(28) \qquad where\ N = \frac{\rho N_A}{M} \#(29)$$

where N_A is Avogadro's number (6.022 × 10^{23} mol^{-1}), ρ is the density of silica (2.2 g·cm^{-3}), M is the molar mass of silica (60.08 g·mol^{-1}), and n is the refractive index of silica at 589 nm (1.4585). The surface molecular density N_a of silica was obtained from the diameter d_a, assuming a layer of O^{2-} ions tightly packed on the surface (a common assumption in the case of adsorption on oxides), such that:

$$N_a = \frac{1}{d_a^2} \#(30)$$

DR method: To confirm the microporous volume value obtained using the HK method (although it is less precise than the latter, especially when the microporous volume is significant), the Dubinin-Radushkevich (DR) equation was used. This equation is an extension of the Polanyi potential theory, which states that molecules near a surface are subjected to a potential field[10]. The adsorbate on the surface is in a liquid state, and its local pressure is inversely equal to the vapor pressure at the adsorption temperature[10]. The DR equation is expressed as follows[10]:

$$\frac{V}{V_t} = \exp\left(\frac{-RT\ln\left(\frac{P}{P_0}\right)}{\epsilon}\right)^2 \#(31)$$

where V is the volume of adsorbed gas (m³), V_t is the total volume of adsorbed gas (m³), and ε is the characteristic adsorption energy (J·mol⁻¹). To obtain the total microporous volume, the equation must first be linearized:

$$\ln(V) = \ln(V_t) - \left(\frac{RT}{\epsilon}\right)^2 ln^2\left(\frac{P}{P_0}\right) \#(32)$$

By plotting $\ln(V)$ as a function of $[ln(P / P_0)]^2$ and performing a linear regression of the form $y = ax + b$, the intercept can be used to calculate the total microporous volume:

$$V_{micro} = \frac{\exp(b) v_m^l}{v_m} \#(33)$$

where V_{micro} is the total microporous volume (cm³·g⁻¹), b is the intercept from the previous equation, v_m^l is the molar volume of liquid N_2 at 77 K (34.7 cm³·mol⁻¹), and v_m is the molar volume of the adsorbed gas (22400 cm³·mol⁻¹).

References

1 M. Thommes, K. Kaneko, A. V. Neimark, J. P. Olivier, F. Rodriguez-Reinoso, J. Rouquerol, K. S. W. Sing, *Pure and Applied Chemistry*, 2015, **87**, 1051–1069.

2 F. Rouquerol, J. Rouquerol, I. Beurroies, P. Llewellyn, R. Denoyel, *Techniques de l'Ingénieur*, 2017, 1–22.

3 F. Rouquerol, J. Rouquerol, I. Beurroies, P. Llewellyn, R. Denoyel, *Techniques de l'Ingénieur*, 2017, 1–20.

4 G. Horváth, K. Kawazoe, *Journal of Chemical Engineering of Japan*, 1983, **16**, 470–475.

5 L. S. Cheng, R. T. Yang, *Adsorption*, 1995, **1**, 187–196.

6 R. W. Baker, Membrane Technology and Applications, 2012, Wiley.

7 L. S. Cheng, Y. Ralph T, *Chemical Engineering Science*, 1994, **49**, 2599–2609.

8 S. U. Rege, R. T. Yang, *AIChE Journal*, 2000, **46**, 734–750.

9 W. M. Haynes, D. R. Lide, T. J. Bruno, CRC handbook of chemistry and physics: a ready-reference book of chemical and physical data, 2016, CRC Press.

10 B. P. Bering, M. M. Dubinin, V. V. Serpinsky, *Journal of Colloid and Interface Science*, 1966, **21**, 378–393.